



Investigation of Air Turbulence Intensity Effect on the Flame Structure in Different Flame Holder Geometry

S. A. Hashemi^a, N. Hajjaligol*^a, K. Mazaheri^b, A. Fattahi^a

^a Department of Mechanical Engineering, University of Kashan, Kashan, Iran

^b Department of Mechanical Engineering, University of Tarbiat Modarres, Tehran, Iran

PAPER INFO

Paper history:

Received 25 April 2012

Received in revised form 26 January 2013

Accepted 18 April 2013

Keywords:

Flame Holder

Stabilization

Co-flowing Methane Flame

Turbulence Diffusion Flame

Turbulence Intensity

β -PDF Mode

ABSTRACT

In this paper, the effect of air turbulence intensity on the flame structure in various radii and lengths of a flame holder numerically studied. Finite volume method is used to solve the governing equations. The obtained numerical results using realizable k - ϵ and β -PDF models show a good agreement with the experimental data. The results show that the flame holders with greater lengths yield shorter flame lengths and higher flame temperature. Also, it is observed that by increasing flame holder radius, flame length slightly decreases at first, and then it increases. When holder radius increases, flame temperature increases first and decreases thereafter. The results indicate that increasing air turbulence intensity results in considerable decrease in flame length, flame temperature, NO formation and temperature gradient in the flame zone.

doi: 10.5829/idosi.ije.2013.26.12c.03

1. INTRODUCTION

Flame stabilization is one of the most important aspects of burner design. Stabilization may be occurred by means of a recirculation zone which returns hot gases to the unreacted mixture. Using hot gases, the recirculation zone plays the role of an igniter [1]. There are some ways for creating a recirculation zone such as using swirl vanes and a central bluff body or inserting a step. Swirl flows have been widely used by investigators due to their numerous applications in the combustion. Olivani et al. [2] experimentally studied the near field flow structure of two swirl stabilized non-premixed flames formed at the end of two concentric pipes with no quarl cone. It was observed that the direction of fuel injection plays an important role on mixture formation and flame stabilization in the recirculation zone.

Using a bluff body is another method to stabilize high-speed flows. Influences of drag coefficients and analysis of wake aerodynamics on stability boundaries

were studied by Herbert [3]. He revealed that stabilization is aided by wakes. Tankin et al. [4] studied the bluff-body effect on the bluff-body stabilized flame combustor and concluded that central jet having higher momentum than air jet, penetrated through recirculation zone and affected its size. Later on, a numerical investigation of the blockage ratio effect on the jet mixing was carried out by Ma and Harn [5]. It was argued that intensity of the recirculation increased with its cone angle.

Some researchers studied the capabilities of combustion models in simulating the turbulent reacting flows. Soong and Chang [6] surveyed various presumed PDF models including the double δ function, the clipped Gaussian function and the β function. These models were studied using two averaging methods, Favre and Reynolds. They have demonstrated that the averaging method is more important in affecting the simulation results compared to the type of presumed PDF model. Kyne et al. [7] compared the results of PDF and laminar flamelet combustion models with experimental data in an air-spray combustor. They also compared two different turbulence models including k - ϵ and Reynolds Stress in their combustor geometry. They could not

*Corresponding Author Email: Najmeh.Hajjaligol@gmail.com (N. Hajjaligol)

clearly explain the differences between velocity fields from the two models. Repp et al. [8] utilized a presumed PDF and a Monte Carlo model in a swirling diffusion flame. They concluded that the accuracy of the two models is the same. However, the computation time for the Monte Carlo model is about 9 times more than that of the PDF model. Guo et al. [9] noticed that the presumed PDF model has advantages over the other models such as Arrhenius, eddy break-up (EBU)-Arrhenius, and laminar flamelet based on comparison with experimental data for a turbulent flame.

Recently, the effect of free stream turbulence on the structure of CH₄-air flames was reported by Saqr et al. [10]. The turbulence intensity of airstream supplied to the flame region was found to affect the shape and size of the reaction zone significantly, inducing flame extinguish at elevated values. According to the literature review, many researchers used different ways for flame stabilization. According to the authors' knowledge, there is no open literature discussing the concept of effect of wall as a conventional flame holder. Thus, the current study aims to investigate the effect of air turbulence intensity on the flame structure in various radii and lengths of a flame holder. Finite volume method as well as k-ε turbulence and β-PDF combustion models are used to solve the governing equations and predict the effect of air turbulence intensity on the flame structure. In this study, FLUENT commercial software is used. The model is validated via several test problems [11].

2. EXPERIMENTAL SETUP

In this investigation, an experimental setup as shown in Figure 1 was prepared in order to validate the numerical results. It consists of air and fuel supply systems, thermocouples, control PC and burner setup with a flame holder. The air supply system is composed of a tank of air, a flow control valve and a calibrated rotameter. The fuel supply system consists of a flow control valve and an electronic flow meter. To ensure the desired accuracy of the measured values, the rotameter and flow meter were calibrated before each measurement using reference gases. Air and fuel enter at ambient temperatures (about 300 K). The fuel and air are injected from two independent channels and are mixed in the burner. The burner temperature was controlled by the temperature programming control device with B-type thermocouples. The accuracy of the rotameters and flow meter was ±3% and that of thermocouples ±2% of recorded value. The experimental repeatability on recorded temperature was ±2%. Since the temperature of flame holder affects the results, and in order to reach a steady state condition, the burner was set to work two hours before starting the measurements.

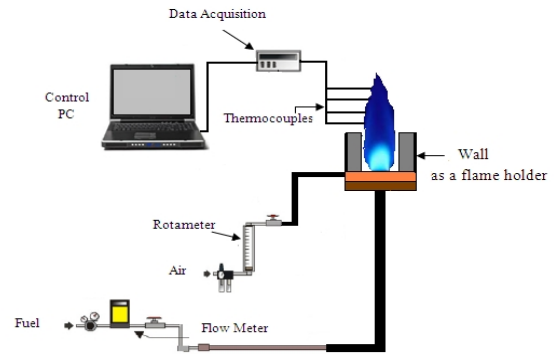


Figure 1. Experimental setup

3. GOVERNING EQUATIONS

Conservative equations for a steady-state reacting flow are used here. A generalized equation describing overall mass, momentum, energy and chemical species concentration is described as [12]:

$$\sum_i \frac{\partial}{\partial x_i} (\rho V_i \phi) = \sum_i \frac{\partial}{\partial x_i} (\Gamma_\phi \frac{\partial \phi}{\partial x_i}) + S_\phi \quad (1)$$

where ϕ is the general variable. Equation (1) yields conservation equation of mass, momentum, energy and species mass fraction when ϕ is one, velocity component, enthalpy and mass fraction respectively. S_ϕ is the source term in the conservation equations. For brevity, the individual equations are not discussed here.

4. TUBULENCE MODEL

The realizable k-ε turbulence model [13] is applied in this study. In comparison with the standard k-ε, this model hinders the negation of values of the normal Reynolds stresses by employing a new turbulent eddy viscosity formulation. It also utilizes a new transport equation for dissipation rate, which hires different sink and source terms. Because of some disadvantages of the standard k-ε turbulence model, some researchers proposed the realizable model for diffusion flames [11, 14, 15]. Further details of the realizable k-ε turbulence model can be found in [13]. Turbulence intensity is expressed as:

$$I = \frac{V'}{V_{avr}} = \sqrt{\frac{\frac{2}{3}k}{u^2 + v^2}} \quad (2)$$

5. TUBULENCE-COMBUSTION INTERACTION

Because of the fluctuating characteristics of a turbulent mixing process, the Probability Density Function is a

professional method for the cases including combustion process and turbulent flow. β -PDF model is used in this study due to its better results for the turbulent non-premixed reacting flow in comparison with the other PDF models [16]. In this model, two parameters of the mean scalar quantity and its variance define the PDF. In the presumed β -PDF model, because of difficulty in solving the transport equation for each species, the mixture fraction, \bar{f} is defined in terms of mass fraction of specie i , Y_i :

$$\bar{f} = \frac{Y_i - Y_{i,ox}}{Y_{i,f} - Y_{i,ox}} \quad (3)$$

where subscripts “ f ” and “ ox ” denote fuel and oxidant species, respectively. The transport equations of mean mixture fraction, \bar{f} and its variance, $\overline{f'^2}$ are:

$$\frac{\partial}{\partial t}(\rho\bar{f}) + \frac{\partial}{\partial x_j}(\rho u_j \bar{f}) = \frac{\partial}{\partial x_j} \left(\frac{\mu_i}{\sigma_i} \frac{\partial \bar{f}}{\partial x_j} \right) \quad (4)$$

$$\frac{\partial}{\partial t}(\rho\overline{f'^2}) + \frac{\partial}{\partial x_j}(\rho u_j \overline{f'^2}) = \frac{\partial}{\partial x_j} \left(\frac{\mu_i}{\sigma_i} \frac{\partial \overline{f'^2}}{\partial x_j} \right) + C_g \mu_i \left(\frac{\partial \bar{f}}{\partial x_j} \right)^2 - C_d \rho \frac{\varepsilon}{k} \overline{f'^2} \quad (5)$$

in which the constant values of σ_i , C_g and C_d are 0.85, 2.86 and 2.0, respectively. The relation between the obtained time-averaged values from the above equations and the instantaneous mixture fraction is established by a PDF model. This function is written as $p(f)$, which demonstrates the probability that the fluid is in the vicinity of state f . The method applies to mean values of species concentration and temperature. The mean mass fraction of species and temperature, $\bar{\phi}_i$, is calculated as:

$$\bar{\phi}_i = \int_0^1 p(f) \phi_i(f) df \quad (6)$$

where, $p(f) = \frac{f^{\alpha-1}(1-f)^{\beta-1}}{\int_0^1 f^{\alpha-1}(1-f)^{\beta-1} df}$; α and β are defined

as follows:

$$\alpha = \bar{f} \left[\frac{\bar{f}(1-\bar{f})}{\overline{f'^2}} - 1 \right] \quad (7)$$

$$\beta = (1-\bar{f}) \left[\frac{\bar{f}(1-\bar{f})}{\overline{f'^2}} - 1 \right] \quad (8)$$

For the non-adiabatic case, the mean enthalpy transport equation is described as:

$$\frac{\partial}{\partial t}(\rho\bar{h}) + \nabla \cdot (\rho\bar{v}\bar{h}) = \nabla \cdot \left(\frac{k_p}{c_p} \nabla \bar{h} \right) \quad (9)$$

Chemical equilibrium is used for determining the product mole fractions.

6. GEOMETRY AND BOUNDARY CONDITIONS

Figure 2 shows the geometry of the burner model. The radius of fuel inlet (R_f) and the radius of air inlet (R_a) of

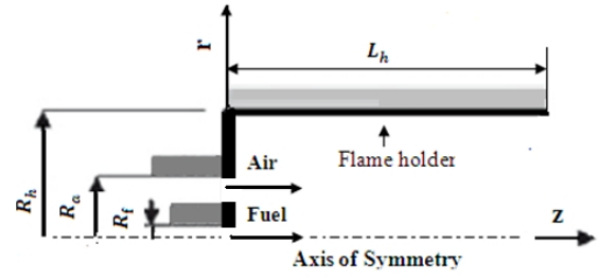


Figure 2. Burner configuration.

the coaxial burner are 0.003 m and 0.011 m, respectively. In the cases of study, the length of flame holder and radius possess different values. Holder length (L_h) varies from 100 mm to 200 mm and holder radius (R_h) changes from 21.5 mm to 31.5 mm.

The velocity of fuel and air are 5.9 m/s and 6.8 m/s respectively. The fuel is pure methane. Air turbulence intensity (ATI) changes from 15 to 55%. The inlet air turbulence kinetic energy and its dissipation rate are expressed as [12]:

$$k = \frac{3}{2} (U_{ref} I)^2 \quad \varepsilon = 0.16 \frac{k^{1.5}}{\ell} \quad (10)$$

In which I , ℓ , U_{ref} are turbulence intensity, characteristic length and inlet velocity respectively. The characteristic length, ℓ , is defined as [12]:

$$\ell = 0.07 L_h \quad (11)$$

The burner exit pressure is 1 bar. Due to the symmetry, one half of the longitudinal section of physical model is simulated. The boundary conditions are as follows:

At burner inlet ($z=0$):

$$r < R_f: \rho = \rho_f, \quad T = T_f, \quad v = 0, \quad u = u_f, \quad Y_i = Y_{f,i}, \quad i = 1, 2, \dots, n \quad (12)$$

$$R_f < r < R_a: \rho = \rho_a, \quad T = T_a, \quad v = 0, \quad u = u_a, \quad Y_i = Y_{a,i}, \quad i = 1, 2, \dots, n \quad (13)$$

At outlet ($0 < r < 5R_h$ and $z = 0.5m$):

$$v = 0, \quad \frac{\partial u}{\partial z} = 0, \quad \frac{\partial Y_i}{\partial z} = 0, \quad \frac{\partial T}{\partial z} = 0, \quad i = 1, 2, \dots, n \quad (14)$$

At burner axis of symmetry ($r=0$):

$$v = 0, \quad \frac{\partial u}{\partial z} = 0, \quad \frac{\partial Y_i}{\partial r} = 0, \quad \frac{\partial T}{\partial r} = 0, \quad \frac{\partial p}{\partial r} = 0, \quad i = 1, 2, \dots, n \quad (15)$$

At the flame holder ($r=R_h$):

$$z < L_h, \quad u = 0, \quad v = 0, \quad \frac{\partial Y_i}{\partial r} = 0, \quad \frac{\partial T}{\partial r} = 0, \quad i = 1, 2, \dots, n \quad (16)$$

At $R_h < r < 5R_h$:

$$z = L_h, \quad v = 0, \quad \frac{\partial u}{\partial z} = 0, \quad \frac{\partial Y_i}{\partial z} = 0, \quad \frac{\partial T}{\partial z} = 0, \quad i = 1, 2, \dots, n \quad (17)$$

At $r=5R_h$:

$$L_h < z < 0.5m: \frac{\partial u}{\partial r} = 0, v = 0, \frac{\partial Y_i}{\partial r} = 0, \frac{\partial T}{\partial r} = 0, i = 1, 2, \dots, n \quad (18)$$

7. NUMERICAL PROCEDURE

The governing nonlinear equations together with the boundary conditions are solved by iterative numerical approach using the finite volume method [17] and a second order upwind scheme to discretize the equations. In order to couple the velocity field and pressure in the momentum equations, the well-known SIMPLE (Semi-Implicit Method for Pressure-Linked Equations) algorithm is used. The convergence criterion of the numerical method is chosen as the total normalized residuals being less than 10^{-6} for each conservative equation. The various grid sizes for the case of ATI=15% are examined to obtain the optimal grid size. The grid is denser near the inlet zone due to the mixing and reaction processes. To obtain a grid-independent solution, various grids (16,320, 23,450, 29,700, 35,600 and 40,100 cells) are tested for $R_h=31.5$ mm and $L_h=100$ mm. Figure 3 shows temperature profile versus radius in axial location $z=0.1$ m. Based on the figure, the grid including 35,600 cells is appropriate to ensure a grid-independent solution.

8. NO_x FORMATION

NO_x formation is an important topic in combustion processes because of its considerable contribution to air pollution. NO is the most important species in NO_x emission for many types of flames [18]. Due to low NO mole fraction, NO_x formation process does not have an important effect on the flow field; hence, it is post processed from the simulation [19].

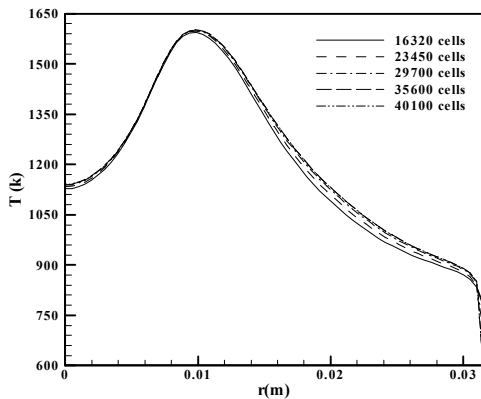


Figure 3. Radial distribution of temperature for $z=0.1$ m at $L_h=100$ mm and $R_h=31.5$ mm: Grid independent.

To include NO formation in this type of flame, the thermal and prompt mechanisms are employed [19] and calculated by finite rate chemistry. The following transport equation is only required for these two mechanisms:

$$\frac{\partial}{\partial t}(\rho Y_{NO}) + \nabla \cdot (\rho \vec{v} Y_{NO}) = \nabla \cdot (\rho D \nabla Y_{NO}) + S_{NO} \quad (19)$$

in which Y_{NO} , D and S_{NO} are NO mass fraction, effective diffusion and the source term respectively. S_{NO} can be calculated as follows:

$$S_{NO} = M_{w,NO} \left(\frac{d[NO]}{dt} \right) \quad (20)$$

where $M_{w,NO}$ is the molecular weight of NO and $\frac{d[NO]}{dt}$ is calculated by both thermal and prompt mechanisms. The thermal NO formation rate is determined according to the highly temperature-dependent reactions referred to as the extended Zeldovich mechanism [18]. Assuming a quasi-steady-state for concentration of nitrogen atoms, the thermal NO formation rate becomes:

$$\frac{d[NO]}{dt} = 2k_1[O][N_2] \frac{(1 - \frac{k_{-1}k_{-2}[NO]^2}{k_1[N_2]k_2[O_2]})}{(1 + \frac{k_{-1}[NO]}{k_2[O_2] + k_3[OH]})} \quad (21)$$

in which the reaction rate coefficients are:

$$k_1 = 1.8 \cdot 10^8 \exp(-38370/T) \text{ [m}^3/\text{kmol}\cdot\text{s]}, \\ k_{-1} = 3.8 \cdot 10^7 \exp(-425/T), k_2 = 1.8 \cdot 10^4 T \exp(-4680/T), \\ k_{-2} = 3.81 \cdot 10^3 T \exp(-20820/T) \text{ and} \\ k_3 = 7.1 \cdot 10^7 \exp(-450/T) \text{ [20].}$$

According to partial equilibrium calculation, the concentration of O atoms is obtained as follows [21]:

$$[O] = 36.64 T^{0.5} [O_2]^{0.5} \exp(-27123 / T) \quad (22)$$

The prompt NO formation rate is obtained by the following equation [22]:

$$\frac{d[NO]}{dt} = f_c k_{prompt} [O_2]^\alpha [N_2] [fuel] \exp\left(\frac{E_a}{RT}\right) \quad (23)$$

in which, α is the order of reaction and f_c is a correction factor which depends on the fuel type and fuel air ratio. The values of k_{prompt} and E are $6.4 \cdot 10^6$ and 72500 cal/gr respectively.

9. MODELS VALIDATION

In order to validate the numerical model for the present case, the solution is compared with the experimental data. Note that the model is validated with several test problems [11]. Figure 4 represents the comparison between numerical results and experimental data at centerline of the burner ($r=0$ and $0 < z < 0.5$ m) for a flame holder with $R_h = 31.5$ mm and $L_h = 100$ mm. The

temperature rises from a minimum at the inlet to a maximum value and then mitigates towards the outlet. Figure 5 shows the comparison for radial temperature at $z=0.14$. As shown in Figures 4 and 5, the values and locations of peak temperature for the experimental and numerical results are approximately the same. The trend of the temperature profile in both results is similar. In spite of some differences, the numerical results are in a good agreement with the experimental data.

10. RESULTS AND DISCUSSION

In this section, the effect of changing ATI in various flame holder radii and lengths on flame structure is studied. For $L_h=100$ mm and $R_h=31.5$ mm, the isotherms when $ATI=15\%$ are shown in Figure 6(a). As the figure shows, a thin flame zone with high temperature is created in the burner, while the temperature in the other zones is almost constant. For $ATI=55\%$, the temperature gradient is not high in a special zone as shown in Figure 6(b). The pattern of the isotherms is almost homogenous.

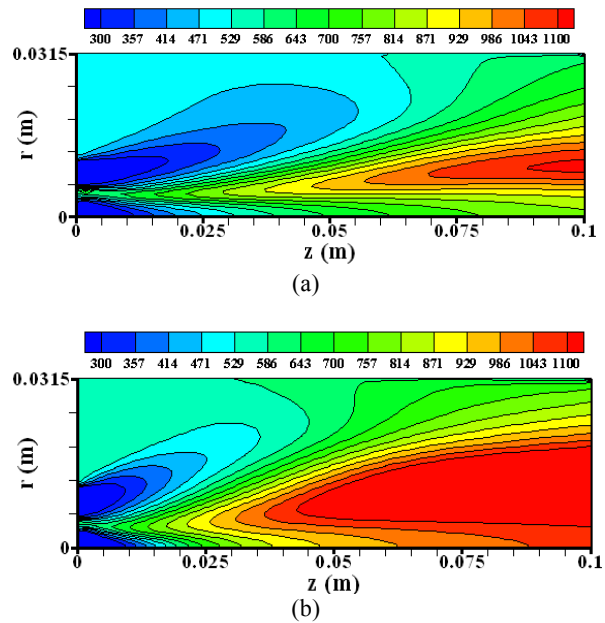


Figure 6. Temperature distribution [K] in the burner for at $L_h=100$ mm and $R_h=31.5$ mm (a) $ATI=15\%$ (b) $ATI=55\%$.

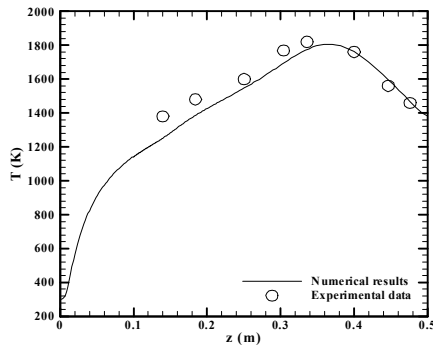


Figure 4. Axial distribution of temperature for $r=0$ at $L_h=100$ mm and $R_h=31.5$ mm: comparison between numerical results and experimental data.

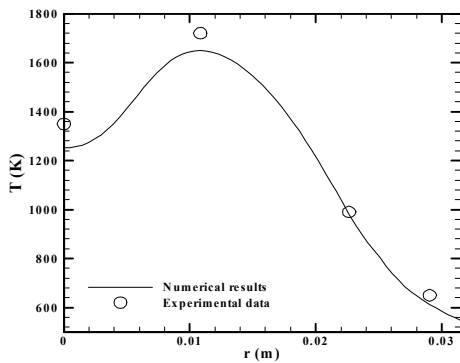


Figure 5. Radial distribution of temperature for $z=0.14$ m at $L_h=100$ mm and $R_h=31.5$ mm: comparison between numerical results and experimental data.

Figure 7 shows flame length versus ATI in three radii of the holder. The holder length for all cases is $L_h=100$ mm. There are different definitions for flame length. For numerical simulations the location of maximum temperature gradient, stoichiometric line and maximum OH concentration are considered as a flame length. In experimental works, flame luminescence and maximum OH concentration are the well-known definitions for flame length [23]. Flame length is defined as the axial distance from the flame base to the farthest point of the flame tip [24]. The maximum OH concentration is adopted as a flame length. Figure 7 reveals that flame length of the holder with middle radius ($R_h=26.5$) is minimum. To explain what is happening, attention to Figure 8 and Table 1 is needed. The recirculation zone returns hot gases to the initial mixture and serves as a preheat source as illustrated in Figure 8. Table 1 demonstrates the mass flow rate of hot gases that come near the reactant by the recirculation zone (obtained in the top half zone of the recirculation zone). Mass flow rate is calculated by Equation (24):

$$\dot{m} = \psi_{max} - \psi_{min} \tag{24}$$

The mass flow rates in Table 1 are for $ATI=15\%$ and $L_h=100$ mm. As the table shows, mass flow rate is maximum for middle radius ($R_h=26.5$). As a result, the behavior of flame length is mainly affected by the mass flow rate of returned hot gases. It is obvious that flame length significantly decreases with increasing the air turbulence intensity (ATI). The decrease in flame length is more noticeable at $R_h=26.5$. As ATI increases from 15% to 55%, the flame length decreases more than 40%

for $R_h=21.5$, 95% for $R_h=26.5$ and more than 16% for $R_h=31.5$.

Flame length versus ATI in three lengths of the holder and $R_h=31.5$ mm is illustrated in Figure 9. As revealed in Figure 9, by increasing L_h the flame length decreases. Table 2 shows mass flow rate of returned hot gases by the recirculation zone for various L_h , $R_h=31.5$ mm and $ATI=15\%$. As the table shows, the increase of the flame holder length increases mass flow rate. According to these results, changing the flame length with L_h is logical. This figure shows that flame length decreases with increasing ATI similar to Figure 7. The decrease is significant when $L_h=200$ mm. As ATI is changed from 15% to 55%, reduction in flame length is 16% for $L_h=100$ mm, while the reduction is 26% when $L_h=150$ mm and is about 92% for $L_h=200$ mm. In all flame holder lengths, the decrease of flame length has almost a linear trend.

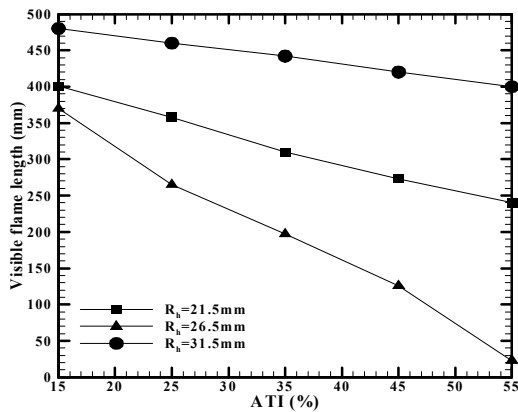


Figure 7. Flame length versus ATI for three holder radii ($L_h=100$ mm).

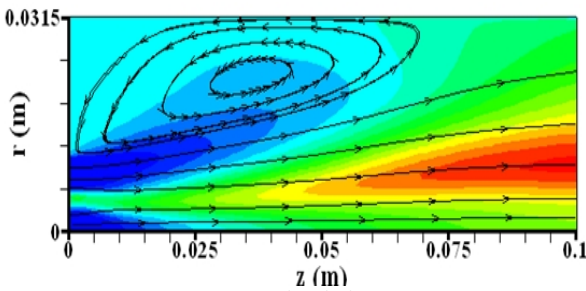


Figure 8. Recirculation zone.

TABLE 1. Mass flow rate of returned hot gases in the top half of the recirculation zone for $L_h=100$ mm and various R_h ($ATI=15\%$).

| R_h (mm) | 21.5 | 26.5 | 31.5 |
|----------------------|-------|-------|-------|
| Mass flow rate (g/s) | 0.393 | 0.421 | 0.292 |

TABLE 2. Mass flow rate of returned hot gases in the top half of the recirculation zone for $L_h=100$ mm and various R_h ($ATI=15\%$).

| L_h (mm) | 100 | 150 | 200 |
|----------------------|-------|-------|-------|
| Mass flow rate (g/s) | 0.292 | 0.325 | 0.356 |

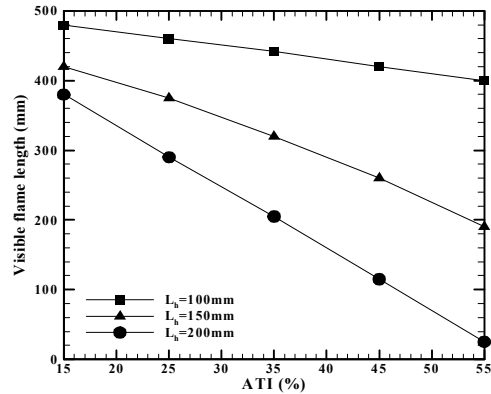


Figure 9. Flame length versus ATI for three holder lengths ($R_h=31.5$ mm).

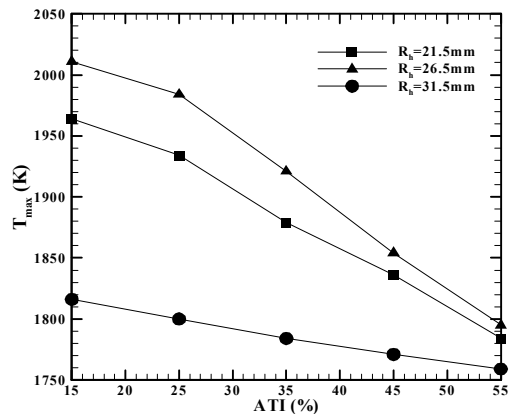


Figure 10. Maximum temperature versus ATI for three holder radii ($L_h=100$ mm).

Figure 10 shows maximum temperature in the burner for different holder radii, five ATIs and $L_h=100$ mm. It is clear that increasing ATI decreases the maximum temperature. As mentioned before, due to the recirculation zone, burnt gases come near the unburnt gases in the burner entrance. With increasing ATI, more blending of the burnt and unburnt gases takes place [23]. Then, the temperature of hot gases decreases due to the high heat capacity of the unburnt gases. It can be observed that maximum temperature in $R_h=26.5$ mm is higher than that of the two other radii at all ATIs. As ATI increases from 15% to 55%, the maximum temperature decreases more than 9% for $R_h=21.5$, 11% for $R_h=26.5$ and more than 3% for $R_h=31.5$.

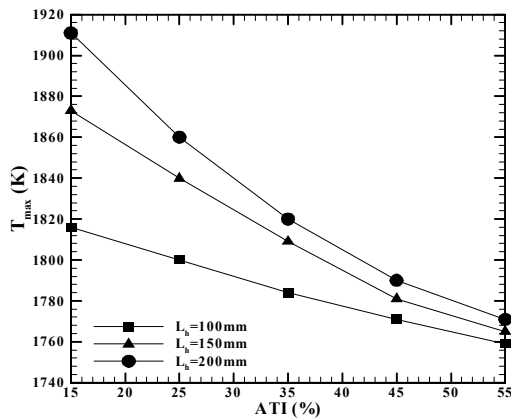


Figure 11. Maximum temperature versus ATI for three holder lengths ($R_h=31.5$ mm).

Maximum temperature in the burner for three lengths of the holder, five ATIs and $R_h=31.5$ mm is illustrated in Figure 11. This figure shows that for all holder lengths with increasing ATI, maximum temperature decreases similar to Figure 10. Figure 11 indicates that for three lengths, maximum temperature increases by increasing L_h . Figure 11 also confirms that the flame temperature of $L_h=200$ mm has higher slip than another value of holder lengths. As ATI is changed from 15% to 55%, reduction of flame temperature is 3% for $L_h=100$ mm, while the reduction is 5.7% when $L_h=150$ mm and is about 7.3% for $L_h=200$ mm.

Pollution emission is an important aspect of a burner and it is discussed here. Table 3 shows averaged NO concentration (ppm) and mass fraction of CO at the

outlet of the holder with $L_h=100$ mm in various R_h and ATIs. NO concentration ($[NO]$) is calculated by a mass-averaged integral at the burner outlet. $[NO]$ and CO mass fraction (Y_{CO}) show very similar trends with flame temperature in these cases. It is obvious that $[NO]$ and Y_{CO} significantly decrease with increasing ATI. To explain what is happening attention to Figure 6 is needed. As shown in Figure 6, at ATI=15%, the high temperature gradient in a thin zone may result in increasing $[NO]$. This pattern is not seen at ATI=55% and temperature gradient is almost identical in the burner. Hence, the NO_x concentration cannot significantly increase. The maximum $[NO]$ and Y_{CO} in all ATIs occurs in $R_h=26.5$ mm. When ATI increases from 15% to 55%, $[NO]$ decreases about 32% for $R_h=21.5$, 38% for $R_h=26.5$ and about 30% for $R_h=31.5$. In these cases, reduction in Y_{CO} is 11% for $R_h=21.5$ mm, while it is 16% for $R_h=26.5$ mm and 4% for $R_h=31.5$ mm.

Averaged NO concentration (ppm) and mass fraction of CO at the outlet of holder length at $R_h=31.5$ mm in various L_h and ATIs are shown in Table 4. $[NO]$ and Y_{CO} show very similar trend with flame temperature in these cases too. The maximum $[NO]$ and CO for all the fuel occur in $L_h=200$ mm. As ATI is changed from 15% to 55%, reduction in $[NO]$ is 30% for $L_h=100$ mm, while the reduction is 42% when $L_h=150$ mm and is about 50% for $L_h=200$ mm. Reduction in Y_{CO} is 4% for $L_h=100$ mm, while it is 13% for $L_h=150$ mm and 20% for $L_h=200$ mm.

TABLE 3. Averaged NO concentration (ppm) and mass fraction of CO at the outlet of the flame holder with $L_h=100$ mm and various R_h and ATIs.

| | | ATI (%) | | | | |
|--------------|----------|---------|---------|---------|---------|---------|
| | | 15 | 25 | 35 | 45 | 55 |
| NO_x (ppm) | 21.5 | 37 | 35 | 33 | 29 | 25 |
| | Y_{CO} | 0.00164 | 0.00156 | 0.00151 | 0.00149 | 0.00146 |
| NO_x (ppm) | 26.5 | 44 | 39 | 36 | 31 | 27 |
| | Y_{CO} | 0.00178 | 0.00171 | 0.00163 | 0.00154 | 0.00149 |
| NO_x (ppm) | 31.5 | 30 | 28 | 27 | 24 | 21 |
| | Y_{CO} | 0.00147 | 0.00146 | 0.00145 | 0.00142 | 0.00141 |

TABLE 4. Averaged NO concentration (ppm) and mass fraction of CO at the outlet of the flame holder with $R_h=31.5$ mm and various L_h and ATIs.

| | | ATI (%) | | | | |
|--------------|----------|---------|---------|---------|---------|---------|
| | | 15 | 25 | 35 | 45 | 55 |
| NO_x (ppm) | 100 | 30 | 28 | 27 | 24 | 21 |
| | Y_{CO} | 0.00147 | 0.00146 | 0.00145 | 0.00142 | 0.00141 |
| NO_x (ppm) | 150 | 39 | 37 | 33 | 27 | 22 |
| | Y_{CO} | 0.00168 | 0.00163 | 0.00154 | 0.00149 | 0.00145 |
| NO_x (ppm) | 200 | 48 | 45 | 36 | 29 | 24 |
| | Y_{CO} | 0.00191 | 0.00185 | 0.00169 | 0.00162 | 0.00152 |

11. CONCLUSION

A validated numerical simulation with the experimental data is used to investigate the effect of air turbulence intensity on the flame structure in various radii and lengths of a flame holder. The results are listed briefly as follows:

1. The validated numerical simulation can well predict the non-premixed flame parameters as compared to the experimental data.
2. Regardless of ATI, the increase of the flame holder radii from $R_h=21.5$ – to 26.5mm decreases the flame length and increases maximum temperature. From $R_h=26.5$ – to 31.5mm, flame length increases and maximum temperature decreases. The effect of ATI is more in $R_h=26.5$ mm.
3. Increasing the flame holder length decreases flame length and increases the maximum temperature in the burner regardless of ATI percents. The effect of ATI is more in longer flame holder length.
4. When ATI increases from 15% to 55%, flame length, flame temperature, Averaged NO concentration (ppm) and mass fraction of CO at the outlet of holder length decreases. More reduction of these parameters occurs in $R_h=26.5$ mm with constant holder length and in $L_h=200$ mm with constant holder radius.
5. The analysis shows that the increasing air turbulence intensity results in decreasing [NO] formation and temperature gradient in the flame zone.

12. REFERENCES

1. Williams, G. C., Hottel, H. and Scurlock, A. C., "Flame stabilization and propagation in high velocity gas streams", in Symposium on Combustion and Flame, and Explosion Phenomena, Elsevier. Vol. 3, (1949), 21-40.
2. Olivani, A., Solero, G., Cozzi, F. and Coghe, A., "Near field flow structure of isothermal swirling flows and reacting non-premixed swirling flames", *Experimental Thermal and Fluid Science*, Vol. 31, No. 5, (2007), 427-436.
3. Herbert, M., "Aerodynamic influences on flame stability", *Progress in Combustion Science and Technology*, VI, (1960), 61-109.
4. Roquemore, W., Tankin, R., Chiu, H. and Lottes, S., "A study of a bluff-body combustor using laser sheet lighting", *Experiments in Fluids*, Vol. 4, No. 4, (1986), 205-213.
5. Ma, H. and Harn, J., "The jet mixing effect on reaction flow in a bluff-body burner", *International Journal of Heat and Mass Transfer*, Vol. 37, No. 18, (1994), 2957-2967.
6. Soong, H. and Chang, K., "Examination of interactions between turbulence and combustion in diffusion flame", *International Journal of Turbo Jet Engines*, Vol. 9, (1992), 227-238.
7. Kyne, A., Pourkashanian, M., Wilson, C. and Williams, A., "Validation of a flamelet approach to modelling 3-d turbulent combustion within an airspray combustor", ASME. (2002).
8. Repp, S., Sadiki, A., Schneider, C., Hinz, A., Landefeld, T., and Janicka, J., "Prediction of swirling confined diffusion flame with a monte carlo and a presumed-pdf-model", *International Journal of Heat and Mass Transfer*, Vol. 45, No. 6, (2002), 1271-1285.
9. Guo, Z., Zhang, H., Chan, C. and Lin, W., "Presumed joint probability density function model for turbulent combustion", *Fuel*, Vol. 82, No. 9, (2003), 1091-1101.
10. Saqr, K., Sies, M. and Wahid, M., "Numerical investigation of the turbulence-combustion interaction in nonpremixed CH₄/air flames", *International Journal of Applied Mathematics and Mechanics*, Vol. 5, No. 8, (2009), 69-79.
11. A, H. S., A, F., A, S. G. and A., M. M., "Investigation of the effect of air turbulence intensity on nox emission in non-premixed hydrogen and Hydrogen-hydrocarbon composite fuel combustion", *International Journal of Hydrogen Energy*, Vol. 36, (2011), 10159-10169.
12. Versteeg, H. K., "An introduction to computational fluid dynamics the finite volume method, 2/e", Pearson Education India, (1995).
13. Shih, T.-H., Liou, W. W., Shabbir, A., Yang, Z. and Zhu, J., "A new k- ϵ eddy viscosity model for high reynolds number turbulent flows", *Computers & Fluids*, Vol. 24, No. 3, (1995), 227-238.
14. Lopez-Parra, F. and Turan, A., Computational study on the effect of turbulence intensity and pulse frequency in soot concentration in an acetylene diffusion flame, in Computational science-ICCS, Springer, (2005), 120-128.
15. Poinso, T. and Veynante, D., "Theoretical and numerical combustion", RT Edwards Incorporated, (2005).
16. Ilbas, M., Yilmaz, İ. and Kaplan, Y., "Investigations of hydrogen and hydrogen-hydrocarbon composite fuel combustion and nox emission characteristics in a model combustor", *International Journal of Hydrogen Energy*, Vol. 30, No. 10, (2005), 1139-1147.
17. Lopez-Parra, F. and Turan, A., "Computational study on the effects of non-periodic flow perturbations on the emissions of soot and NO_x in a confined turbulent methane/air diffusion flame", *Combustion Science and Technology*, Vol. 179, No. 7, (2007), 1361-1384.
18. Drake, M., Correa, S., Pitz, R., Shyy, W. and Fenimore, C., "Superequilibrium and thermal nitric oxide formation in turbulent diffusion flames", *Combustion and Flame*, Vol. 69, No. 3, (1987), 347-365.
19. Jiang, B., Liang, H., Huang, G. and LI, X., "Study on NO_x formation in CH₄/air jet combustion", *Chinese Journal of Chemical Engineering*, Vol. 14, No. 6, (2006), 723-728.
20. Hanson, R. K. and Salimian, S., Survey of rate constants in the N/H/O system, in Combustion chemistry, Springer, (1984) 361-421.
21. Raine, R., Stone, C. and Gould, J., "Modeling of nitric oxide formation in spark ignition engines with a multizone burned gas", *Combustion and Flame*, Vol. 102, No. 3, (1995), 241-255.
22. De Soete, G. G., "Overall reaction rates of no and N₂ formation from fuel nitrogen", in Symposium (international) on combustion, Elsevier. Vol. 15, No., (1975), 1093-1102.
23. Turns, S. R., "An introduction to combustion", McGraw-Hill New York, Vol. 499, (1996).
24. Oh, J. and Yoon, Y., "Flame stabilization in a lifted non-premixed turbulent hydrogen jet with coaxial air", *International Journal of Hydrogen Energy*, Vol. 35, No. 19, (2010), 10569-10579.

Investigation of Air Turbulence Intensity Effect on the Flame Structure in Different Flame Holder Geometry

S. A. Hashemi^a, N. Hajialigol^a, K. Mazaheri^b, A. Fattahi^a

^a Department of Mechanical Engineering, University of Kashan, Kashan, Iran

^b Department of Mechanical Engineering, University of Tarbiat Modarres, Tehran, Iran

PAPER INFO

چکیده

Paper history:

Received 25 April 2012

Received in revised form 26 January 2013

Accepted 18 April 2013

Keywords:

Flame Holder

Stabilization

Co-flowing Methane Flame

Turbulence Diffusion Flame

Turbulence Intensity

β -PDF Mode

این مطالعه به بررسی اثر شدت آشفته‌گی هوای ورودی در ابعاد مختلف نگه‌دارنده‌ی شعله بر ساختار شعله‌ی غیرپیش‌آمیخته می‌پردازد. از دینامیک سیالات محاسباتی به عنوان ابزار این مطالعه استفاده شده است. به همین دلیل پیش از بررسی پارامترهای مورد نظر نسبت به اعتباردهی نتایج با استفاده از داده‌های تجربی معتبر اقدام شده است. از روش β -PDF برای مدل‌سازی احتراق و از مدل $k-\epsilon$ تحقیق‌پذیر برای مدل‌سازی آشفته‌گی جریان استفاده شده است. مشاهده شد که افزایش طول نگه‌دارنده‌ی شعله، منجر به کاهش طول شعله، افزایش دمای بیشینه و افزایش غلظت اکسیدهای نیتروژن خواهد شد. همچنین، نتایج نشان داد که برای سه شعاع مختلف نگه‌دارنده‌ی شعله‌ی مورد بررسی، کمترین طول شعله و بالاترین دمای بیشینه برای شعاع متوسط رخ می‌دهد. به علاوه، ملاحظه شد که با افزایش شدت آشفته‌گی هوای ورودی، طول شعله، دمای بیشینه و اکسیدهای نیتروژن تولیدی کم خواهند شد. بیشترین اثر شدت آشفته‌گی هوا بر ساختار شعله در بزرگ‌ترین طول و شعاع متوسط نگه‌دارنده‌ی شعله اتفاق می‌افتد.

doi: 10.5829/idosi.ije.2013.26.12c.03

